Adaptive Algorithms for Active Sound-Profiling

Lewis E. Rees and Stephen J. Elliott, *Senior Member, IEEE*

***Abstract*—Three novel adaptive algorithms are proposed for use in active sound-profiling, all based on the filtered-X least mean square (FXLMS) approach. The algorithms are analyzed for their stability properties and control effort load, and are compared with the currently used adaptive noise equalizer least mean square (ANE-LMS) algorithm. It is found that the most suitable algorithm, both in simulations and experimentally, is the phase scheduled command FXLMS (PSC-FXLMS), which possesses both low control effort and good stability in the face of plant model misestimation, especially when using an automatic phase command law.**

***Index Terms*—Active noise control (ANC), active sound-profiling, adaptive noise equalizer (ANE), command-FXLMS, filtered-X least mean square (FXLMS), internal model FXLMS, PSC-FXLMS.**

I. Introduction

THE use of active noise control (ANC) in the automobile industry has been discussed for some years, but with few real applications making it to the production line [1]. One novel use of active control that is currently being investigated is known as active sound-profiling, which is used to change the amplitude of engine orders to improve engine sound quality. This process, which is similar to ANC, uses adaptive algorithms to change the coefficients of a set of digital filters such that not only are some selected frequencies cancelled by a loudspeaker generating an inverse disturbance signal, but others are controlled to a predetermined level or even enhanced. Typically the output of a microphone is controlled so that its spectrum at a number of discrete frequencies, corresponding to engine orders, is similar to some prescribed target spectrum, which has previously been designed to enhance the subjective sound quality of the car, e.g., by jury tests [2]. Kuo [3], [4] suggests the use of an algorithm; known as the *adaptive noise equalizer* (ANE) for this task, which is a derivative of the filtered-X least mean square (FXLMS) algorithm [5] commonly used in active noise control [6], [7]. The ANE offers complete control over the disturbance signal, for cancellation, attenuation and enhancement. However, the ANE is very sensitive to misestimations in the plant model at high system gains, as described below. This instability was the motivation behind the work in this paper, of which the aim was to design a novel adaptive algorithm that possesses the same control abilities as Kuo's ANE, but with improved stability properties.

Manuscript received June 2, 2004; revised November 5, 2004. This work was supported by Jaguar Cars, Ltd. The associate editor coordinating the review of this manuscript and approving it for publication was Dr. Shoji Makino.

The authors are with the Institute of Sound and Vibration, University of Southampton, Southampton SO17 1BJ, U.K. (e-mail: ler@isvr.soton.ac.uk).

Digital Object Identifier 10.1109/TSA.2005.855828

This paper describes several different approaches to active sound-profiling, for the simple example of a single pure disturbance tone of the form $d(n) = D\cos(\omega_r T n + \phi_d)$, where D is the amplitude of the disturbance signal, ω_r is the reference frequency, $1/T$ is the sample rate, n is the current sample and ϕ_d is the phase of the disturbance signal. This feedforward method of active sound profiling assumes that temporal information is available as a reference signal, most likely from an engine speed measurement, in the form $x(n) = X\cos(\omega_r T n + \phi)$ which is used to drive the digital filters, where X is the amplitude of the reference signal. Multiple frequencies can be controlled by the superposition of several such filters.

In the standard FXLMS, an error signal taken from a microphone in the car cabin, which measures the residual sum of the disturbance signal and the control signal, is used to adapt the weights to minimize the squared value of the error signal. The error signal can be written as

$$e(n) = d(n) + \mathbf{g}^{\mathrm{T}}\mathbf{u}(n) \tag{1}$$

where $e(n)$ is the value of the error signal at sample n, $\mathbf{g}^{\mathrm{T}}$ is a row vector containing the coefficients of the impulse response of the plant between the control loudspeaker and error microphone, and $\mathbf{u}(n)$ is a column vector of previous values of the control signal. The FXLMS update equation used to adapt the filter weights takes the form

$$\mathbf{w}(n+1) = \mathbf{w}(n) - \alpha\hat{\mathbf{r}}(n)e(n) \tag{2}$$

where $\mathbf{w}(n+1)$ and $\mathbf{w}(n)$ are column vectors of the new and current filter weight coefficients, $\hat{\mathbf{r}}(n)$ is a column vector of reference signal values that have been filtered through an estimate model of the plant response, and α is the convergence coefficient, which dictates the rate at which the optimum weights are achieved.

II. Command-FXLMS Algorithm

In active sound profiling of engine noise the requirement is to enhance the gain of certain engine orders, as well as reducing others to tailor a unique engine sound. This technique can be formulated as requiring the error signal, $e(n)$ to tend toward a given command value, $c(n)$, instead of zero. The command signal provides a measure of the target spectrum at that single frequency. The command signal is created from the reference signal, which ensures that its frequency components are the same as those of the disturbance signal and could, for example, be scheduled on the engine speed and load. This leads to the command-FXLMS algorithm, whose block diagram is shown in Fig. 1, for which the update equation becomes

$$\mathbf{w}(n+1) = \mathbf{w}(n) - \alpha\hat{\mathbf{r}}(n)e'(n) \tag{3}$$

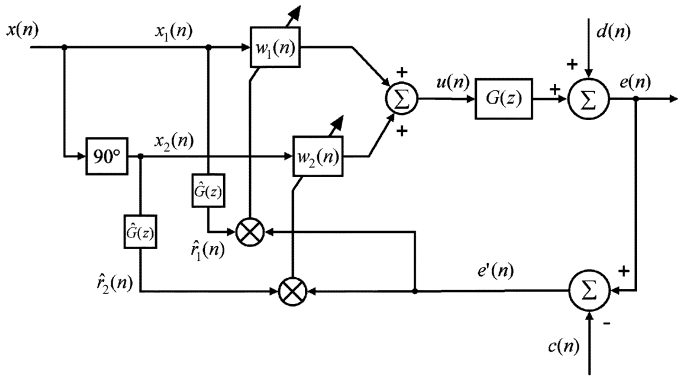

Fig. 1. Block diagram showing the single frequency command-FXLMS algorithm, in which the physical error signal, $e(n)$, tends to the command signal, $c(n)$, as the pseudoerror $e'(n)$ is driven to zero.

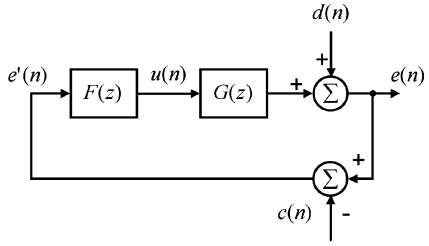

Fig. 2. Alternative block diagram for the command-FXLMS algorithm, containing the transfer function $F(z)$.

where the pseudoerror is $e'(n) = e(n) - c(n)$. As the pseudoerror is driven to zero by the adaptive algorithm $e(n)$ will tend to $c(n)$.

Quadrature reference signals $x_1(n)$ and $x_2(n)$ are assumed, each passing through a single weight, $w_1(n)$ or $w_2(n)$. The transfer function of the plant response, from control loudspeaker to error microphone, is denoted $G(z)$, and the internal model of the plant response used to update the controller is denoted $\hat{G}(z)$. In this case $\mathbf{w}(n) = [w_1(n)\ w_2(n)]^{\mathrm{T}}$ and $\hat{\mathbf{r}}(n) = [\hat{\mathbf{g}}^{\mathrm{T}}\mathbf{x}_1\ \hat{\mathbf{g}}^{\mathrm{T}}\mathbf{x}_2]^{\mathrm{T}}$, where $\mathbf{x}_1$ and $\mathbf{x}_2$ contain past values of $x_1(n)$ and $x_2(n)$, and $\hat{\mathbf{g}}$ is the impulse response of $\hat{G}(z)$.

A. Equivalent Transfer Function and System Stability

It was shown by Glover in 1977 [8] that the response of the time-varying LMS algorithm for the adaptive noise cancellation of a tone, using two reference signals 90° out of phase, could be completely represented by an equivalent closed loop transfer function. This theory, which was extended by Elliott *et al.* to the case of the FXLMS [9], allows Fig. 1 to be redrawn as a closed loop block diagram as in Fig. 2, from which we can see that

$$E(z) = \left[\frac{1}{1 - F(z)G(z)}\right] D(z) - \left[\frac{F(z)G(z)}{1 - F(z)G(z)}\right] C(z) \tag{4}$$

where $F(z)$ is the transfer function of the LMS subsystem

$$F(z) = \frac{U(z)}{E'(z)} = -\alpha\hat{G}\left[\frac{z\cos(\omega_r T - \Phi) - \cos\Phi}{z^2 - 2zcos(\omega_r T) + 1}\right] \tag{5}$$

where $\hat{G}$ and Φ are the magnitude and phase, respectively, of the plant response estimate at the normalized reference frequency $\omega_r T$.

As with the FXLMS, the transfer function from the disturbance signal to the error signal for the complete system $H(z)$ is equal to $E(z)/D(z)$ [9]. In the ideal, case when the command and disturbance signals are in phase and therefore related by a simple gain such that $C(z) = AD(z)$, $H(z)$ is given by (6), as shown at the bottom of the page.

The stability properties of the command-FXLMS under conditions of slow convergence can be determined by examining the poles of (6), as α tends to zero. Under conditions of very slow convergence the dynamic behavior of $G(z)$ is unimportant and $G(z)$ can be arbitrarily set equal to its amplitude at the reference frequency, G, since without loss of generality the phase response can be set to zero, so that Φ is now the phase error in $\hat{G}(z)$. The poles of (6) then form a conjugate pair a distance of $(1 - \alpha G\hat{G}\cos\Phi)^{1/2}$ away from the origin [9]. The system is thus guaranteed to be stable under conditions of slow convergence provided $\cos\Phi > 0$, ie the phase error between the physical plant and plant model is less than $\pm 90°$ [5]. Provided this phase condition is satisfied no amount of error in the magnitude of the plant model, $\hat{G}$, compared with the plant response, G, will cause the system to become unstable provided α is small enough.

B. Control Effort

The control effort is equal to the mean square value of the control signal, $u(n)$, and is proportional to the loudspeaker power required to drive the pseudoerror signal to zero. As the command signal is equal to the sum of the disturbance signal and the control signal under these conditions, the amplitude of $u(n)$ will vary depending on the difference in phase between $d(n)$ and $c(n)$. The two extremes of this effect are shown in Fig. 3, in which the dashed line shows the amplitude of the observed error signal $e(n)$ and that of the time-varying control effort observed in a simulation of the command-FXLMS when the command signal is out of phase with the disturbance. It is clear that the control system first cancels out the disturbance, so the observed error goes to zero at about the 30th iteration, and then generates an output of the required magnitude and phase. The steady state control effort is then much larger than that required when the disturbance is in phase with the command signal, as shown by the solid line in Fig. 3. This difference in steady state effort can easily be shown from the z-transform of (1) and the definition of

$$H(z) = \frac{z^2 - 2zcos\omega_r T + 1 + A\alpha\hat{G}G(z)\left[z\cos(\omega_r T - \Phi) - \cos\Phi\right]}{z^2 - 2zcos\omega_r T + 1 + \alpha\hat{G}G(z)\left[z\cos(\omega_r T - \Phi) - \cos\Phi\right]} \tag{6}$$

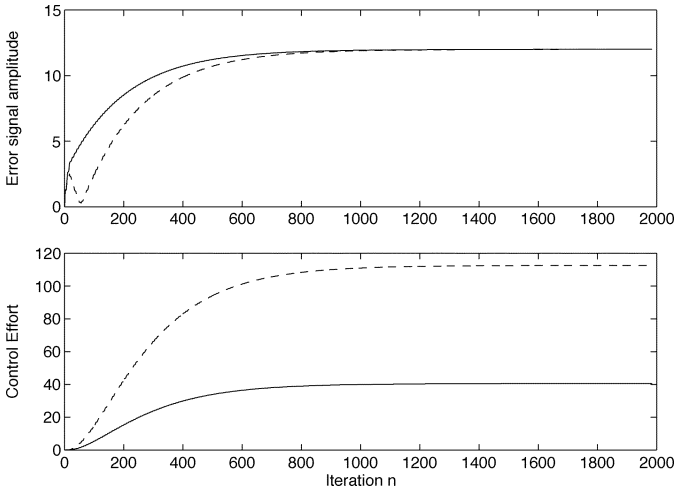

Fig. 3. Time history of the error signal amplitude (upper graph) and control effort (lower graph) for simulations of the command-FXLMS with $\omega_r T = 1/16$, $\alpha = 0.01$, $\hat{G}(z) = G(z) = z^{-16}$, $D = 3$ and $C = 12$, with the command signal in phase with the disturbance signal (solid line) or out of phase (dashed line).

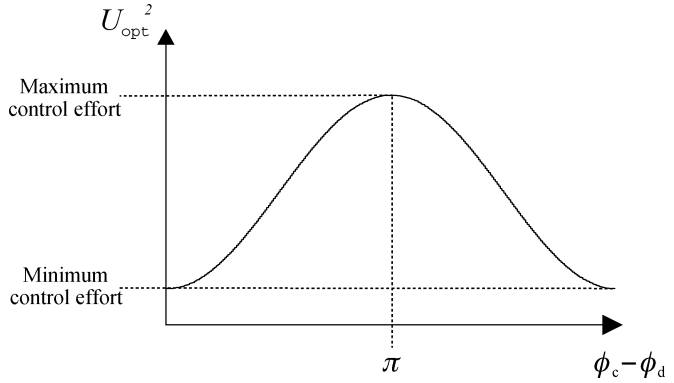

Fig. 4. Variation of the control effort in the command-FXLMS algorithm with the phase difference between the command and disturbance signals.

the pseudoerror, $e'(n)$, which, when set to zero, gives the control signal corresponding to the optimum filter

$$U_{\text{opt}}(z) = \frac{C(z) - D(z)}{G(z)}. \tag{7}$$

Since all the signals are sinusoidal under steady state conditions and defining $|U_{\text{opt}}(e^{j\omega_r T})| = U_{\text{opt}}$, $D(e^{j\omega_r T}) = De^{j\phi_d}$, $C(e^{j\omega_r T}) = Ce^{j\phi_c}$ and $|G(e^{j\omega_r T})| = G$ we can write

$$U_{\text{opt}}^2 = \frac{|Ce^{j\phi_d} - De^{j\phi_c}|^2}{G^2} = \frac{D^2 + C^2 - 2DCcos(\phi_c - \phi_d)}{G^2}. \tag{8}$$

The maximum control effort, of $U_{\text{opt}}^2 = [(C + D)/G]^2$, thus occurs when the disturbance and command signal are out of phase and the minimum, of $U_{\text{opt}}^2 = [(C - D)/G]^2$, occurs when they are in phase, as seen in Fig. 4.

At high values of D this can lead to large amounts of power being wasted, due to a simple phase misalignment of the command signal. In practice the control effort will be limited by the power rating of the loudspeakers used. This will dictate the level of the command signal achievable by the system, which must be calculated under the worst case conditions that the disturbance is out of phase with the command signal.

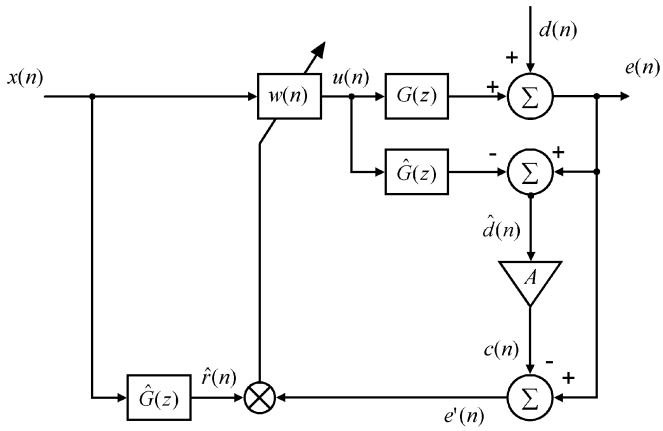

Fig. 5. Block diagram of the internal model FXLMS algorithm.

III. Internal Model FXLMS Algorithm

The internal model FXLMS attempts to limit excessive control effort, by ensuring that the command signal and the disturbance signal are as close in phase as possible. This is done by the addition of an internal model of the plant into the command-FXLMS algorithm. The control signal $u(n)$ is passed through this model of the plant $\hat{G}(z)$ and then subtracted from the error signal $e(n)$ to produce an estimate of the disturbance signal $\hat{d}(n)$; see Fig. 5. This estimate of the disturbance signal is then amplified by the desired command amplification factor A to create the command signal $c(n)$. Provided that the response of the plant model at the reference frequency accurately matches that of the physical plant, the newly created $c(n)$ will be in phase with $d(n)$.

Further analysis of the internal model FXLMS show its similarities to Kuo's ANE-LMS algorithm [3]. From the block diagram in Fig. 5, the pseudoerror equation can be written as

$$e'(n) = e(n) - A\hat{d}(n). \tag{9}$$

Making the substitution

$$\hat{d}(n) = e(n) - \hat{\mathbf{g}}^{\mathrm{T}}\mathbf{u}(n) \tag{10}$$

yields

$$\begin{aligned} e'(n) &= e(n) - A\left[e(n) - \hat{\mathbf{g}}^{\mathrm{T}}\mathbf{u}(n)\right] \\ &= (1 - A)e(n) + A\hat{\mathbf{g}}^{\mathrm{T}}\mathbf{u}(n) \end{aligned} \tag{11}$$

where $\mathbf{g}^{\mathrm{T}}$ and $\hat{\mathbf{g}}^{\mathrm{T}}$ are the transposed vectors of the plant and plant estimate impulse responses respectively, all other variables are as previously noted.

This rearranged form of the error equation leads to a new block diagram, shown in Fig. 6, which bares a close resemblance to the ANE-LMS [3], [4]. The internal model FXLMS now has two branches, as in the ANE-LMS. The minor difference, however, is in the positioning of the amplification blocks, A and $1 - A$. These weight $e(n)$ and the $u(n)$ filtered by the internal model in Fig. 5, but act on $u(n)$ before the plant and the plant model in the ANE-LMS.

A. Equivalent Transfer Function and System Stability

The equivalent transfer function can be used to analyze the stability of the internal model FXLMS. Starting from the block

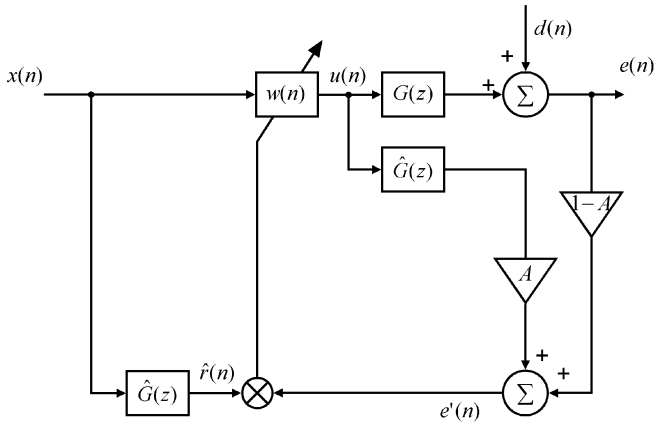

Fig. 6. Alternative block diagram of the internal model FXLMS algorithm, demonstrating the similarity with the ANE-LMS.

diagram in Fig. 5, the error and pseudoerror can be written in the z-domain as

$$E(z) = D(z) + G(z)U(z) \tag{12}$$

$$E'(z) = E(z) - A\hat{D}(z). \tag{13}$$

Rearranging and substituting these equations into the transfer function for $H(z) = E(z)/D(z)$ and using the equivalent transfer function for the LMS update equation $F(z) = U(z)/E'(z)$ yields

$$H(z) = \frac{1 - A\hat{G}(z)F(z)}{1 - G(z)F(z) + A\left[G(z) - \hat{G}(z)\right]F(z)}. \tag{14}$$

The full form for $H(z)$, when $F(z)$ is substituted for (5), is shown in (15). Substituting A for β gives exactly the same form for $H(z)$ as found by Diego *et al.* [10] for the ANE-LMS transfer function. Hence, both algorithms are equivalent and have the same stability properties as in (15), shown at the bottom of the page.

The stability of the internal model FXLMS can now be analyzed by calculating the location of the poles of (15). The poles of the system are calculated by setting the denominator of (15) to zero and solving the resulting quadratic equation in z. If the amplification factor A is zero, (15) reduces to (6) and the algorithm is insensitive to errors in the amplitude of the internal model for slow convergence, provided the phase criteria is satisfied. For nonzero values of A, however, the stability is affected by amplitude errors in $\hat{G}(z)$. This can be illustrated by again assuming that convergence is slow enough to be able to ignore the dynamic behavior of $G(z)$ and $\hat{G}(z)$, and that the plant and plant model possess no phase shift, so that $\Phi = 0$, then $G(z) = G$ and $\hat{G}(z) = \hat{G}$. Hence, the roots of the denominator are

$$z_p = b \pm \sqrt{b^2 + \alpha\hat{G}\left[G - A(G - \hat{G})\right] - 1} \tag{16}$$

where

$$b = \cos\omega_r T - \frac{\alpha}{2}\hat{G}\left[G - A(G - \hat{G})\right]\cos\omega_r T. \tag{17}$$

This can be expressed as

$$z_p = r_p e^{\pm j\phi_p} \tag{18}$$

where the radius of the pole location from the origin of the z-plane is

$$r_p = \sqrt{1 - \alpha\hat{G}\left[G - A(G - \hat{G})\right]} \tag{19}$$

and the angle

$$\phi_p = \cos^{-1}\left[\frac{\cos\omega_r T - \frac{\alpha}{2}\hat{G}\left[G - A(G - \hat{G})\right]\cos\omega_r T}{\sqrt{1 - \alpha\hat{G}\left[G - A(G - \hat{G})\right]}}\right]. \tag{20}$$

The system is stable provided the poles are within the unit circle, which leads to the condition for stability given by

$$\left|1 - \alpha\hat{G}\left[G - A(G - \hat{G})\right]\right| \leq 1. \tag{21}$$

This gives rise to two different conditions for the amplification factor dependent on whether the sum of $G - \hat{G}$ is positive or negative, assuming that α is small these conditions are thus

$$\text{if } \hat{G} < G, \quad A < \frac{G}{G - \hat{G}} \tag{22}$$

$$\text{and if } \hat{G} > G, \quad A < \frac{2}{\alpha\hat{G}(\hat{G} - G)}. \tag{23}$$

As can be seen from (23), the small value of α reduces the constraint on A and thus allows the algorithm to remain stable at higher values of amplification factor when $\hat{G} > G$. However, as will be discussed in the next section, when $\hat{G} > G$ the maximum system gain achievable is reduced. Fig. 7 shows the position of the poles and zeros for a simulation in which various amplification factors are assumed when $\hat{G} = 0.75G$. As the required amplification, A, increases, the poles quickly move outside the unit circle making the system unstable. This makes the internal model FXLMS, like the ANE-LMS, highly susceptible to small changes in the amplitude of the plant response at high system amplifications, which limits the maximum achievable amplification of the system in practice.

B. Amplification Errors of the Internal Model FXLMS

Experimental analysis shows that not only does the difference between the magnitudes of G and $\hat{G}$ affect the stability of the system, but it also directly affects the steady state value of the overall system gain, i.e., the measured value of E/D, where E and D are the magnitudes of the error and disturbance signals, respectively. The optimum control signal for the internal model FXLMS, for which the adaptive filter coefficients are equal to

$$H(z) = \frac{z^2 - 2z\cos\omega_r T + 1 + A\alpha\hat{G}\hat{G}(z)\left[z\cos(\omega_r T - \Phi) - \cos\Phi\right]}{z^2 - 2z\cos\omega_r T + 1 + \alpha\hat{G}\left[G(z) - A\left(G(z) - \hat{G}(z)\right)\right]\left[z\cos(\omega_r T - \Phi) - \cos\Phi\right]} \tag{15}$$

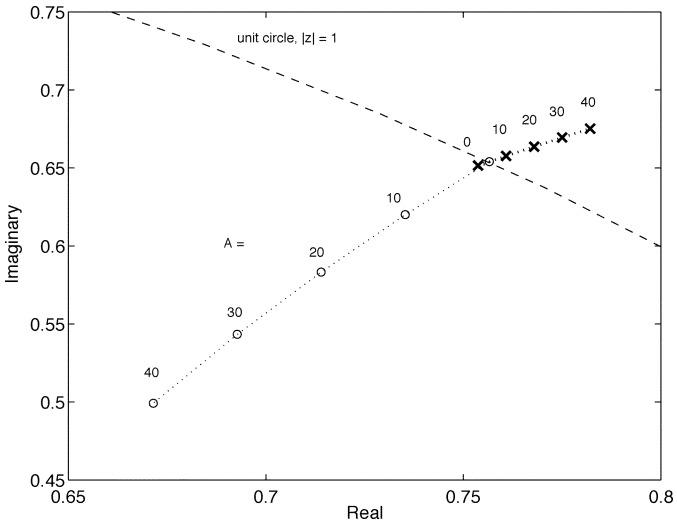

Fig. 7. Plot of part of the complex plane, showing the position of the poles and zeros for the equivalent transfer function of the internal model FXLMS algorithm for amplification factors of $A = 0$, 10, 20, 30, and 40. Other parameters are $\omega_r T = 1/16$, $\alpha = 0.01$, $X = 1$, $D = 3$, and $\hat{G} = 0.75G$.

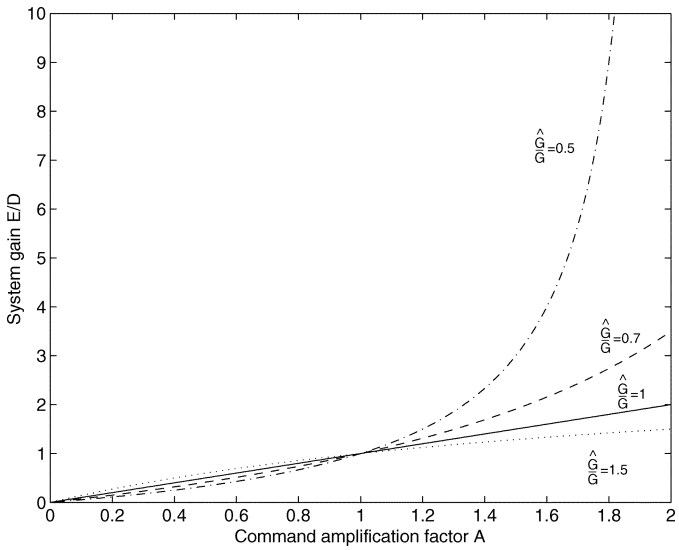

Fig. 8. Graph showing the overall system gain for the internal model FXLMS with increasing amplification factor A for different values of $\hat{G}/G$.

the optimum filter, which drives the pseudoerror to zero, is equal to

$$U_{\text{opt}} = \frac{D(1-A)}{A(G-\hat{G})-G} \tag{24}$$

where it has again been assumed that there is no phase shift in the plant or plant model. The error signal at the microphone is then equal to

$$E = D + U_{\text{opt}}G. \tag{25}$$

After rearranging these equations we find the system gain to be

$$\frac{E}{D} = 1 + \frac{(1-A)}{A\left(1-\frac{\hat{G}}{G}\right)-1}. \tag{26}$$

From (26) it can be seen that the gain of the system is dependent upon the ratio of $\hat{G}/G$ and is only equal to A if $\hat{G} = G$.

Fig. 8 shows the relation between the command amplification factor A and the overall gain of the system for different values of the ratio $\hat{G}/G$. As can be seen from the figure, for values of $\hat{G}/G < 1$ the gain of the system increases sharply for values of A greater than unity. The gain of the system tends to infinity for a value of A governed by the stability condition in (22). In practice, the gain obviously does not reach infinity as A is increased, but goes into an unstable oscillatory state. For $\hat{G}/G = 1$, the gain of the system increases linearly with A as expected. For values of $\hat{G}/G > 1$, in the limit to infinite A, the system gain converges toward a maximum value of

$$\left.\frac{E}{D}\right|_{A=\infty} = 1 - \frac{1}{1-\frac{\hat{G}}{G}}. \tag{27}$$

Therefore, as discussed in the previous section, although (23) states that stability is retained for higher values of A when $\hat{G}/G > 1$, it is usually the case that (27) prevents this system gain from ever being achieved.

This nonlinear behavior of the system gain with the command amplification for the internal model FXLMS algorithm means that any deviation of the physical plant from the plant model will lead to the algorithm converging to an inaccurate system gain. This behavior is exactly the same for the ANE-LMS. Another negative trait of the internal model FXLMS is its inability to produce a nonzero output if the disturbance signal is zero. Even if the disturbance never reaches zero, as observed in practice, the value of A needed to amplify it to a reasonable level will send the internal model FXLMS algorithm into instability with anything but the most accurate of plant estimates.

IV. Phase Scheduled Command-FXLMS Algorithm (PSC-FXLMS)

As seen in Sections II and III the command-FXLMS and the internal model FXLMS both have their strengths and weaknesses. The command-FXLMS is highly robust to amplitude errors in the plant estimate, but has excessive control effort when the command signal is out of phase with the disturbance signal, while the internal model FXLMS is highly sensitive to amplitude errors in the plant model when the command signal is much greater than the disturbance. It is therefore of interest to develop an algorithm that possesses both limited control effort and stability in the face of plant model misestimation.

A new algorithm, known as the phase scheduled command-FXLMS (PSC-FXLMS), is shown in Fig. 9, and has a similar block diagram to the internal model FXLMS. The command signal phase is set by the measured phase of the modeled disturbance, $\hat{d}(n)$, but in this algorithm no amplitude information is transferred from $\hat{d}(n)$ to the command signal, $c(n)$. Instead its amplitude is fixed at an absolute value by a signal generator. This means that any magnitude errors in the estimated plant model have less of an effect on the value of the command signal amplitude, which in turn prevents the instability experienced with the internal model FXLMS.

The phase information, for the alignment of $c(n)$ with $\hat{d}(n)$ is gathered by performing a fast Fourier transform (FFT) on the

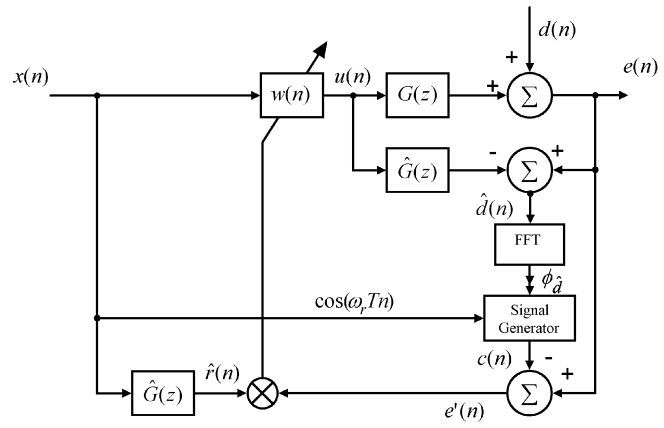

Fig. 9. Block diagram of the phase scheduled command-FXLMS algorithm.

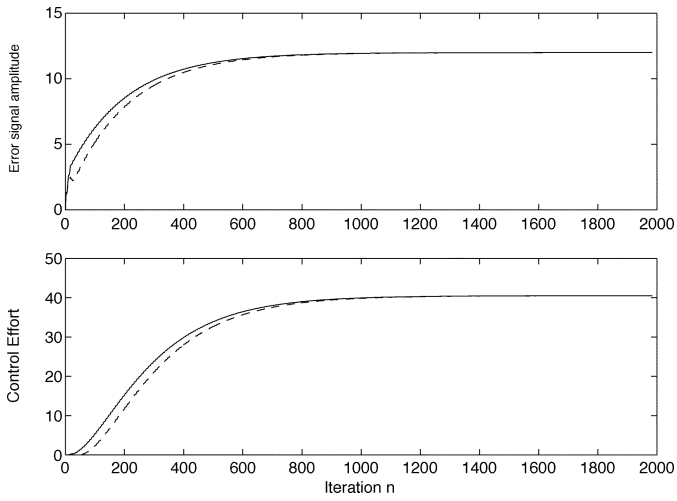

Fig. 10. Time history of the amplitude error signal (upper graph) and control effort (lower graph) for simulations of the PSC-FXLMS with $\omega_r T = 1/16$, $\alpha = 0.01$, $\hat{G}(z) = G(z) = z^{-16}$, $D = 3$, and $C = 12$, with the command signal initially in phase with the disturbance signal (solid line) or out of phase (dashed line).

previous N samples that is assumed to construct one period of the modeled disturbance, and then extracting the phase angle at the frequency corresponding to the reference signal $x(n)$. This FFT is recalculated every N samples to ensure that a phase lock is maintained. Using an FFT to extract the phase information of $\hat{d}(n)$ for a single tone is not necessarily the most computationally efficient method, and may potentially be replaced by a device such as a phase-locked loop circuit to align the phase of $c(n)$ with $\hat{d}(n)$. However, if the PSC-FXLMS was extended to a multifrequency system, only a single FFT would be needed to calculate the phase of $\hat{d}(n)$ for all frequencies requiring control.

The effect of scheduling the command signal phase angle ϕ_c can be seen in Fig. 10, which again shows the time history of the amplitude error signal and control effort. This can be compared with the control effort required for the out of phase command signal for the command-FXLMS in Fig. 3. As long as the plant model is accurate, the minimum control effort for a given command level is achieved.

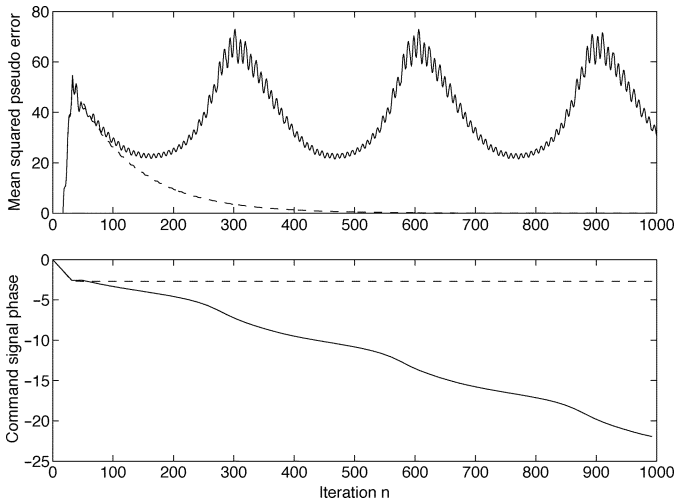

Fig. 11. Phase instability in the PSC-FXLMS, with a small disturbance signal. The dashed line shows the convergence of the algorithm with no phase error, while the solid line shows the instability of the algorithm with a phase error of one sample, i.e., $\pi/8$. $C/D = 10$, $\omega_r T = 1/16$, and $\alpha = 0.01$.

A. Phase Errors in the Plant Estimate

Although the PSC-FXLMS's stability is not affected by magnitude errors between $G(z)$ and $\hat{G}(z)$, it is susceptible to plant estimate phase errors when the commanded amplitude C is large compared with the disturbance amplitude D. The PSC-FXLMS uses an estimate of the disturbance signal $\hat{d}(n)$ to schedule the phase of the command signal $c(n)$. This disturbance estimate is calculated by

$$\begin{aligned}\hat{d}(n) &= e(n) - \hat{\mathbf{g}}^{\mathrm{T}}\mathbf{u}(n) \\ &= d(n) + \left[\mathbf{g} - \hat{\mathbf{g}}\right]^{\mathrm{T}}\mathbf{u}(n)\end{aligned} \tag{28}$$

which, if represented as complex variables at the reference frequency yields

$$\hat{D}e^{j\phi_{\hat{d}}} = De^{j\phi_d} + Ue^{j\phi_u}\left(Ge^{j\phi_g} - \hat{G}e^{j\phi_{\hat{g}}}\right) \tag{29}$$

where $\hat{D}$ and $\phi_{\hat{d}}$ are the magnitude and phase of the disturbance estimate signal, D and ϕ_d are the magnitude and phase of the disturbance signal, U and ϕ_u are the magnitude and phase of the control signal, G and ϕ_g are the magnitude and phase shift of the plant response, and $\hat{G}$ and $\phi_{\hat{g}}$ are the magnitude and phase shift of the plant estimate response.

Equation (29) shows that the phase of $\hat{d}(n)$, and therefore $c(n)$ is dependent not only on that of $d(n)$, but also upon the level of the control signal U and the difference between the physical plant and plant model. Furthermore, $u(n)$ is dependent on $c(n)$, since $u(n) = w(n)x(n)$, and the update equation for a single filter coefficient can be written as

$$\begin{aligned}w(n+1) &= w(n) - \alpha\hat{r}(n)e'(n) \\ &= w(n) - \alpha\hat{r}(n)\left[d(n) + \mathbf{g}^{\mathrm{T}}\mathbf{u}(n) - c(n)\right]\end{aligned} \tag{30}$$

where all variables are as previously stated. This dependence of $c(n)$ on $u(n)$, with a large enough phase error between $G(z)$ and $\hat{G}(z)$ sends the algorithm into a limit cycle, in which $u(n)$ is continuously trying to adapt its phase to cancel $e'(n)$. This change in $u(n)$ causes the phase of $c(n)$ to increase further, and $u(n)$ then tries to adapt to the new phase, but just increases the phase of $c(n)$ once more. Hence, the algorithm never manages to converge and control is lost, as illustrated in Fig. 11.

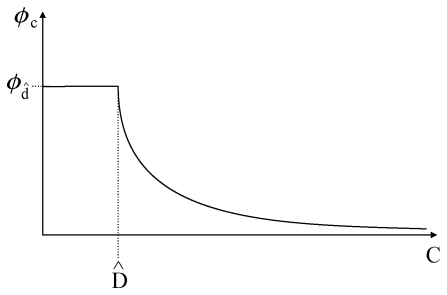

Fig. 12. Function controlling the value of the command signal phase angle ϕ_c, for the APC-FXLMS algorithm, as a function of the level of the command signal C.

The command signal generation part of the PSC-FXLMS, under the ideal situation when $\hat{D}(z) = D(z)$, acts like a perfect automatic gain control system, in which no matter how the input varies the output will always remain the same. This nonlinearity and the complex nature of the command signal production prohibits the valid frequency domain analysis of the algorithm and the derivation of an equivalent transfer function. The lack of an equivalent transfer function makes it difficult to analytically demonstrate the exact cause of the phase instability in the PSC-FXLMS. However, by simulation it can be shown that the phase of the command signal $c(n)$ continuously increases when the system goes unstable, as shown in Fig. 11. This instability puts a limit on the system gain achievable by the PSC-FXLMS.

B. Automatic Phase Command Law (APC-FXLMS)

To deal with the problem of phase instability when large system gains are needed, a technique known as *automatic phase command* has been incorporated into the PSC-FXLMS algorithm. Automatic phase command (APC), is similar to an automatic gain control, and is used to alter the sensitivity of the phase angle of $c(n)$ depending on the disturbance amplification required, as measured by the value of C/D. This derivative of the PSC-FXLMS, known as the APC-FXLMS, controls the phase of the command signal using the following conditions:

$$\text{for } C \leq \hat{D}, \quad \phi_c = \phi_{\hat{d}} \tag{31}$$

$$\text{and for } C > \hat{D}, \quad \phi_c = \frac{2\hat{D}}{\hat{D} + C}\phi_{\hat{d}} \tag{32}$$

where ϕ_c is the phase angle of $c(n)$, $\phi_{\hat{d}}$ is the calculated phase angle of the disturbance estimate and $\hat{D}$ is the amplitude of the disturbance estimate.

As can be seen in Fig. 12, ϕ_c tends toward $\phi_{\hat{d}}$ if C is only slightly greater than $\hat{D}$. For values of the command signal much larger than $\hat{D}$, however, the APC-FXLMS reschedules ϕ_c toward zero. This ensures that for high values of $C/\hat{D}$ the phase angle ϕ_c is less influenced by the second term in (29), and the system remains stable. This modification does result in a slight increase in control effort, for values of C slightly larger than $\hat{D}$, but the increase in control effort becomes negligible as C becomes much larger than $\hat{D}$, since the control system hardly has to cancel any disturbance before generating the command signal.

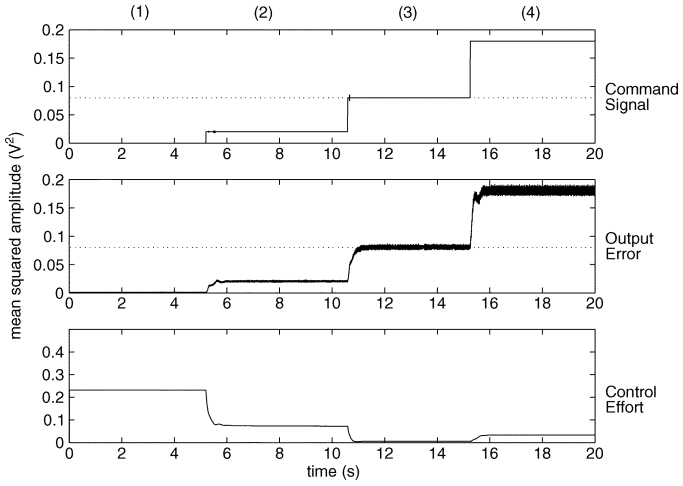

Fig. 13. Experimental results of sound profiling using the PSC-FXLMS algorithm, showing the mean squared command level, $\overline{c^2}(n)$, the error level, $\overline{e^2}(n)$, and the control effort, $\overline{u^2}(n)$. (1)=cancellation mode ($C = 0$), (2)=attenuation mode ($C = 0.5D$), (3)=neutral mode ($C = D$), and (4)=enhancement mode ($C = 1.5D$). The dotted line shows the disturbance signal power level for reference.

V. Experimental Sound Profiling of a Single Tone

A. Using the PSC-FXLMS

Sound profiling of a tone involves four different types of control modes (referred to by Kuo as equalization effects [3]). These are: *Cancellation mode*—when the command level is set to zero, i.e., the PSC-FXLMS acts like the standard FXLMS algorithm, *Attenuation mode*—when the command level is set to a nonzero value lower than the disturbance level, *Neutral mode*—when the command and disturbance levels are set equal, ie no control is necessary, and *Enhancement mode*—when the command level is set to a value greater than the disturbance level.

Experimental results for the sound profiling of a pure 1000 rad^{-1} (159.16 Hz) tone at a sample rate of 16 samples per period (2.55 kHz) in all four modes, using the PSC-FXLMS algorithm, are shown in Fig. 13. The experimental setup involved a two loudspeaker configuration in a short plastic duct. The larger disturbance speaker was located at the rear of the duct, while the smaller control loudspeaker was suspended at the mouth of the duct, thus creating an annular disturbance source with an inner circular secondary source. The control algorithms were implemented on a DSpace DS1103 real-time DSP controller board, which included a 256-tap FIR filter for the plant response model.

The disturbance signal was kept constant for all four modes, while the command signal level, C, was increased in three steps to show the operation of all four modes. The output error level clearly follows the commanded level in all four phases. The control effort is not excessive when the output is enhanced, and is close to zero when the command signal amplitude is the same as that of the disturbance.

B. Stability of the PSC-FXLMS Versus the Internal Model FXLMS

Fig. 14 shows experimental results for the output error for the internal model FXLMS and PSC-FXLMS algorithms in en-

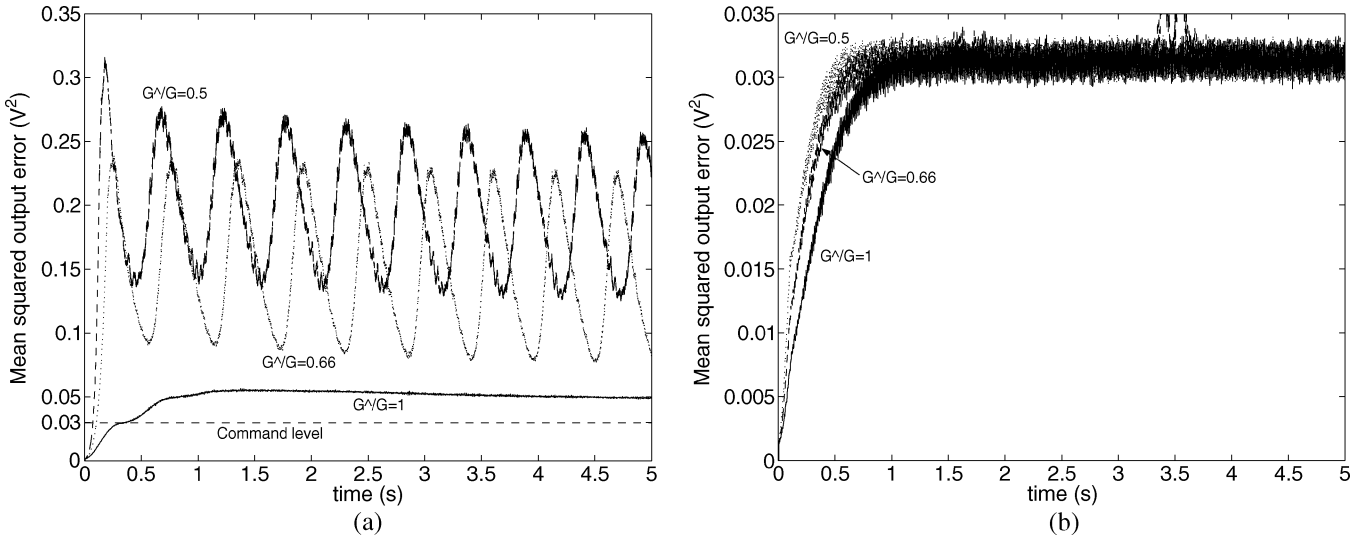

Fig. 14. Comparison of the behavior of the internal model FXLMS and PSC-FXLMS algorithms in enhancement mode. The mean squared output error is shown for plant estimate magnitude errors varying from $\hat{G}/G = 1$ to 0.5, where $\alpha = 0.01$ and the command signal has a mean square value of 0.03 (lower dashed line). Note the difference in scale between the two graphs. (a) Internal model FXLMS, $A = 5$. (b) PSC-FXLMS, $C/D = 5$.

hancement mode, for a system gain of $E/D = 5$ with various deliberately introduced plant model magnitude errors. Fig. 14(a) shows that the internal model FXLMS is unstable, and oscillates with a large amplitude due to saturation effects, for both $\hat{G}/G = 0.5$ and $\hat{G}/G = 0.66$. In theory for $\hat{G}/G = 1$ the algorithm should never go unstable; however, in practice it is impossible to get the plant model to be exactly the same as the plant, and therefore there will always be a practical upper limit to the enhancement of a single tone. Similarly, there will always be a misamplification due to the nonlinear system gain, shown in Fig. 8. In comparison, the PSC-FXLMS converges for all values of $\hat{G}/G$ at $C/D = 5$.

VI. Conclusion

Table I provides a rough qualitative guide to the properties of the various algorithms considered in this paper, including: the speed of convergence, the stability to errors in the plant model, and the amount of control effort required for all phase angles between the disturbance and command signals.

The stability of the algorithms is evaluated separately with respect to both plant estimate errors in magnitude and phase. The most stable of all the algorithms is the command-FXLMS. The command-FXLMS's stability is due to the simplicity of the algorithm, which possesses the same robust properties as the standard FXLMS. Unfortunately it can also have excessive control effort.

The internal model FXLMS is stable at low gains, but due to the amplification of plant model errors with the command signal as the gain increases the stability margin decreases rapidly with amplification ratio, as shown both analytically and experimentally. In practice this results in low achievable system gain, which limits the use of the algorithm in active sound-profiling, specifically when engine orders need to be amplified by a significant amount. The algorithm does, however, require low values of control effort relative to the command-FXLMS. Due to the similarity between the internal model FXLMS and the ANE-LMS, developed by Kuo, the control effort and stability properties hold for both algorithms.

TABLE I
Relative Strengths and Weaknesses of the Algorithms Considered for Active Sound-Profiling

FXLMS Algorithm	Speed	Magnitude Stability	Phase Stability	Control Effort
Command-	Good	Good	Good	Bad
Internal model-	Good	Bad	Fair	Good
PSC-	Good	Good	Fair	Good
APC-	Good	Good	Good	Good/Fair

The PSC-FXLMS has been shown not only to achieve those modes of control capable by the internal model FXLMS with increased gain accuracy, but also with an increase in stability to plant model magnitude errors. Furthermore with the addition of the automatic phase command law, the APC-FXLMS has increased stability to phase errors. The APC-FXLMS's additional stability to phase errors at high system gains results in an increased control effort over the internal model FXLMS, although the difference becomes smaller for larger amplification factors.

Further investigations into the performance and stability of these two algorithms under time varying conditions would be of great use, in particular for applications in the automobile industry. Furthermore, a separate study into the susceptibility of the algorithms to out-of-band overshoot, and the effect that overshoot may have on the effectiveness of the systems is highly important, particularly when dealing with the sound profiling of multiple tones. Overshoot is an effect caused by phase errors in the plant estimate, that results in the amplification of undesirable out-of-band frequencies. Work in this area has been conducted by Kong and Kuo [11] and more recently by Diego *et al.* [10] for Narrow-band ANC systems and a derivative of the ANE algorithm, respectively.

A class of algorithms has thus been developed that offers not only superior stability to the ANE-LMS, but also more flexibility and accuracy in it's amplification of the disturbance signal. These algorithms both converge to a desired system gain

independent of the plant estimate magnitude, and possess the ability to accurately generate a commanded output signal when no disturbance signal is present.

REFERENCES

[1] H. Sano, T. Inoue, A. Takahashi, K. Terai, and Y. Nakamura, "Active control system for low-frequency road noise combined with an audio system," *IEEE Trans. Speech Audio Process.*, vol. 9, no. 7, pp. 755–763, Jul. 2001.

[2] A. Miśkiewicz and T. Letowski, "Psychoacoustics in the automotive industry," *Acustica*, vol. 85, no. 5, pp. 646–649, 1999.

[3] S. M. Kuo and M. J. Ji, "Development and analysis of an adaptive noise equaliser," *IEEE Trans. Speech Audio Process.*, vol. 3, no. 3, pp. 217–222, May 1995.

[4] S. M. Kuo and D. R. Morgan, *Active Noise Control Systems: Algorithms and DSP Implementation*. New York: Wiley, 1996.

[5] D. R. Morgan, "An analysis of multiple correlation cancellation loops with a filter in the auxiliary path," *IEEE Trans. Acoust., Speech, Signal Process.*, vol. ASSP-28, no. 4, pp. 454–467, 1980.

[6] J. C. Burgess, "Active adaptive sound control in a duct: A computer simulation," *J. Acoust. Soc. Amer.*, vol. 70, no. 3, pp. 715–726, 1981.

[7] P. A. Nelson and S. J. Elliott, *Active Control of Sound*. New York: Academic, 1992.

[8] J. R. Glover, Jr., "Adaptive noise canceling applied to sinusoidal interferences," *IEEE Trans. Acoust., Speech, Signal Process.*, vol. ASSP-25, no. 6, pp. 484–491, Jun. 1977.

[9] S. J. Elliott, I. M. Stothers, and P. A. Nelson, "A multiple error lms algorithm and its application to the active control of sound and vibration," *IEEE Trans. Acoust., Speech, Signal Process.*, vol. 35, no. 10, pp. 1423–1434, Oct. 1987.

[10] M. de Diego, A. Gonzalez, M. Ferrer, and G. Piñero, "Performance comparison of multichannel active noise control equalizers," in *Proc. Active 2002*, 2002, pp. 413–423.

[11] X. Kong and S. M. Kuo, "Analysis of asymmetric out-of-band overshoot in narrow-band active noise control systems," *IEEE Trans. Speech Audio Process.*, vol. 7, no. 5, pp. 587–591, Sep. 1999.

Lewis E. Rees was born in Leicester, U.K., in 1979. He received the M.Sci. honors degree in physics from Imperial College, London, U.K., and the Ph.D. degree in active noise control of automobiles from the Institute of Sound and Vibration Research, University of Southampton, Southampton, U.K., in 2001 and 2005, respectively.

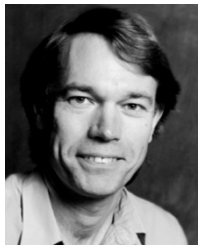

Stephen J. Elliott (SM'92) graduated in physics and electronics from the University of London, London, U.K., in 1976 and received the Ph.D. degree from the University of Surrey, Surrey, U.K., in 1979 for a dissertation on musical acoustics.

After a short period as a Research Fellow at the Institute of Sound and Vibration Research (ISVR) working on acoustic intensity measurement and as a temporary Lecturer at the University of Surrey, he was appointed Lecturer at ISVR, University of Southampton, in 1982. He was made Senior Lecturer at ISVR in 1988 and Professor in 1994. His research interests have been mainly concerned with the connections between the physical world and digital signal processing, originally in relation to the modeling and synthesis of speech and, more recently, in relation to the active control of sound and vibration. This work has resulted in the practical demonstration of active control in propeller aircraft, cars, and helicopters. His current research interests include the active control of structural waves, active isolation, adaptive algorithms for feedforward and feedback control, and biomedical signal processing and control.

Dr. Elliot was jointly awarded the Tyndall Medal from the Institute of Acoustics in 1992 and the Kenneth Harris James Prize from the Institution of Mechanical Engineers in 2000. He is a member of the Acoustical Society of America.